


ARTICLE

Open Access

# The central role of tilted anisotropy for field-free spin-orbit torque switching of perpendicular magnetization

Chen-Yu Hu<sup>1</sup>, Wei-De Chen<sup>1</sup>, Yan-Ting Liu<sup>1</sup>, Chao-Chung Huang<sup>1</sup> and Chi-Feng Pai<sup>1,2,3</sup> 

## Abstract

The discovery of efficient magnetization switching upon device activation by spin Hall effect (SHE)-induced spin-orbit torque (SOT) changed the course of magnetic random-access memory (MRAM) research and development. However, for electronic systems with perpendicular magnetic anisotropy (PMA), the use of SOT is still hampered by the necessity of a longitudinal magnetic field to break magnetic symmetry and achieve deterministic switching. In this work, we demonstrate that robust and tunable field-free current-driven SOT switching of perpendicular magnetization can be controlled by the growth protocol in Pt-based magnetic heterostructures. We further elucidate that such growth-dependent symmetry breaking originates from the laterally tilted magnetic anisotropy of the ferromagnetic layer with PMA, a phenomenon that has been largely neglected in previous studies. We show experimentally and in simulation that in a PMA system with tilted anisotropy, the deterministic field-free switching exhibits a conventional SHE-induced damping-like torque feature, and the resulting current-induced effective field shows a nonlinear dependence on the applied current density. This relationship could be potentially misattributed to an unconventional SOT origin.

## Introduction

The ultrafast and energy-efficient characteristics of employing spin-orbit torque (SOT)<sup>1–3</sup> for magnetization switching make it a promising writing mechanism for next-generation magnetic random-access memory (MRAM)<sup>4,5</sup>. In various types of magnetic heterostructures, by applying an in-plane current ( $J_c \parallel \hat{x}$ ) through spin current sources (SCSs), such as bulk materials with a sizable spin Hall effect (SHE)<sup>6–8</sup> or interfaces with a strong Rashba effect<sup>9,10</sup>, the generated spin current with transverse polarization ( $\sigma \parallel \hat{y}$ ) transfers spin angular momentum to the neighboring magnetization ( $M$ ) and then activates magnetic dynamics. Such spin-torque-induced dynamics of  $M$  can be described by the

Landau-Lifshitz-Gilbert-Slonczewski (LLGS) equation<sup>11,12</sup> comprised of a field-like (FL-) and a damping-like (DL-) SOT term, where  $\tau_{FL} \propto M \times \sigma$  and  $\tau_{DL} \propto M \times (\sigma \times M)$ . Considering scalability and stability<sup>13</sup>, magnetic heterostructures with perpendicular magnetic anisotropy (PMA) are deemed the best candidates for SOT-MRAM applications. However, such applications are limited by the symmetry of SOT<sup>2</sup>, such that either  $\tau_{DL}$  or  $\tau_{FL}$  cannot provide the necessary symmetry breaking between the UP and DOWN state of the magnetic materials (FM) with PMA, which leads to a non-deterministic SOT switching behavior. To break the symmetry and realize the deterministic SOT switching, the simplest approach is to apply an in-plane field along the current direction ( $H \parallel \hat{x}$ )<sup>14–16</sup>, which has been demonstrated by introducing a magnetic hard mask (MHM)<sup>17</sup> in the SOT-MRAM cell with PMA. However, a field-free solution is much more desirable for industrial applications.

Correspondence: Chi-Feng Pai (cfpai@ntu.edu.tw)

<sup>1</sup>Department of Materials Science and Engineering, National Taiwan University, Taipei 10617, Taiwan

<sup>2</sup>Center of Atomic Initiative for New Materials, National Taiwan University, Taipei 10617, Taiwan

Full list of author information is available at the end of the article

These authors contributed equally: Chen-Yu Hu, Wei-De Chen

© The Author(s) 2024



**Open Access** This article is licensed under a Creative Commons Attribution 4.0 International License, which permits use, sharing, adaptation, distribution and reproduction in any medium or format, as long as you give appropriate credit to the original author(s) and the source, provide a link to the Creative Commons license, and indicate if changes were made. The images or other third party material in this article are included in the article's Creative Commons license, unless indicated otherwise in a credit line to the material. If material is not included in the article's Creative Commons license and your intended use is not permitted by statutory regulation or exceeds the permitted use, you will need to obtain permission directly from the copyright holder. To view a copy of this license, visit <http://creativecommons.org/licenses/by/4.0/>.

Some commonly studied symmetry breaking mechanisms for achieving field-free SOT switching of a PMA FM layer include tilted magnetic anisotropy (anisotropy gradient<sup>18</sup>, device shape engineering<sup>19</sup>, magneto-crystalline anisotropy<sup>20</sup>, mixed magnetic anisotropy<sup>21,22</sup>), unconventional spin currents (low symmetry materials<sup>23</sup>, magnetic spin Hall effect<sup>24</sup>, competing spin currents<sup>25,26</sup>), perpendicular FL-SOT (oxidation gradient at CoFeB/oxide interface<sup>27</sup>), symmetric<sup>28</sup> and antisymmetric<sup>29</sup> interlayer exchange coupling, exchange bias coupling<sup>30,31</sup>, and the orange peel effect<sup>32</sup>. In addition to the above-mentioned approaches, oblique angle deposition of magnetic heterostructures is another method to introduce structural symmetry breaking in PMA systems, but the corresponding mechanism for field-free switching strongly depends on the stack design and device fabrication process. For example, the lateral magnetic anisotropy asymmetry from the ferromagnetic layer thickness gradient is concluded to be the field-free switching origin for the Pt/Co(obliquely deposited)/MgO structure<sup>16</sup>; the SOT gradient is for the Cu–Pt(obliquely deposited)/[Co/Ni]<sub>n</sub> structure<sup>33</sup>; and the tilted magnetic anisotropy is for the Pt/Co(obliquely deposited)/Pt structure<sup>18</sup> and the heavy-metal(obliquely deposited)/CoFeB(obliquely deposited)/MgO structure<sup>34</sup>. Due to these diverse proposed mechanisms and the lack of a universal and engineering-friendly protocol to realize robust field-free SOT switching, we therefore try to scrutinize the origin of symmetry breaking in a simple PMA system, namely, Pt/Co/Pt trilayer, as-prepared by different oblique deposition approaches. Our experimental and simulated results indicate that tilted magnetic anisotropy is strongly correlated with the oblique deposition angle and the texture transformation of the Pt buffer layer. Field-free switching in such a system can also be explained by a conventional SHE-induced DL-SOT plus tilted magnetic anisotropy effect, in which the inclusions of unconventional spin current or exotic SOT terms are unnecessary.

## Materials and methods

### Sample preparation

We sputter-deposited Ta(0.5)/Pt(5)/Co(0.5)/Pt(1)/Ta(2) (units in nanometers) with PMA on thermally oxidized Si substrates. The bottom Ta(0.5) serves as a seed layer to ensure the uniformity of the films, and the top Ta(2) is expected to be naturally oxidized to prevent other layers from oxidation. The film stacks are prepared in a magnetron sputtering system with a base pressure of  $1 \times 10^{-8}$  Torr and a working pressure of 3 mTorr by Ar gas flow. Hall bar devices with lateral dimensions of  $5 \mu\text{m} \times 60 \mu\text{m}$  and  $10 \mu\text{m} \times 60 \mu\text{m}$  are subsequently patterned for electrical measurements. The oblique angle deposition in this work is achieved by using a wedge-shaped sample holder with different oblique angles and is controlled by the

deposition angle ( $\theta_{\text{dep}}$ ) of the Pt atom flow based on our chamber design. The azimuthal angle of deposition ( $\alpha$ ) is controlled by the placement of the Hall bar pattern on the wedge-shaped holder, as shown in Fig. 1a. For instance, based on the coordinate of the Hall bar device ( $x, y, z$ ), the Pt atom flow originates from the  $-y$  direction of the Hall bar device for the  $\alpha = 0^\circ$  geometry, from the  $-x$  direction for the  $\alpha = 90^\circ$  geometry, and so on. For the control samples prepared with  $\theta_{\text{dep}} = 0^\circ$ , the sample holder rotates during the whole deposition process to avoid wedge effects. At conditions of  $\theta_{\text{dep}} = 20^\circ, 30^\circ, 40^\circ$ , the sample holder remains static during the deposition of the Ta(0.5)/Pt(5) buffer layer to control the direction of the incoming atom flow. Then, sample holder rotation is resumed for depositing the rest of the layers (Co(0.5)/Pt(1)/Ta(2)). The sputtering rate of each material is calibrated for different  $\theta_{\text{dep}}$  conditions by a profilometer. In addition, the thickness gradients of the obliquely deposited Pt layer and uniformly deposited Co prepared using a wedge-shaped holder are confirmed to be negligible in the  $5 \mu\text{m}$ -wide Hall bar devices (see Supporting Information S1).

### Basic electrical and magnetic properties

Electrical measurements on Hall bar devices are performed with a current source (Keithley 2400) and a voltage meter (Keithley 2000) integrated into a probe station with or without electromagnets based on the characterization purpose. The electromagnets are typical home-made coils with iron cores in the case of applying a typical field along the  $x, y, z$ -axis and a commercial projected vector field magnet of model GMW Associates Model 5204 for applying arbitrary vector fields based on the previously established framework<sup>35</sup>. An X-ray diffractometer (XRD) (model Rigaku TTRAX-III) was used to characterize the crystallinity of the deposited films. A vibrating sample magnetometer (MicroSense EZ9 VSM) is used to characterize the saturation magnetization and the dead layer thickness.

The longitudinal resistivities ( $\rho_{xx}$ ) of the Pt and Co layers are obtained by four-point probe measurements and the parallel resistor model, giving  $\rho_{\text{Co}} = 85.32 \mu\Omega \text{ cm}$  and  $\rho_{\text{Pt}} = 18.8 \mu\Omega \text{ cm}$ , and the deposition angle shows a negligible influence on the film resistivity. The VSM characterization results show that the Co layer has a saturation magnetization of  $M_s = 1132.3 \pm 30.9 \text{ emu/cm}^3$  with a negligible dead layer thickness ( $t_{\text{dead}} \sim 0 \text{ nm}$ ). The PMA properties of the magnetic heterostructures prepared under different  $\theta_{\text{dep}}$  are evaluated via typical anomalous Hall effect (AHE) hysteresis measurements<sup>36</sup>, as shown in Fig. 1b. The coercivity ( $H_c$ ) is defined to occur when the normalized Hall resistance ( $R_H$ ) changes its sign as sweeping an out-of-plane magnetic field ( $H_z$ ). The ratio between the remnant perpendicular

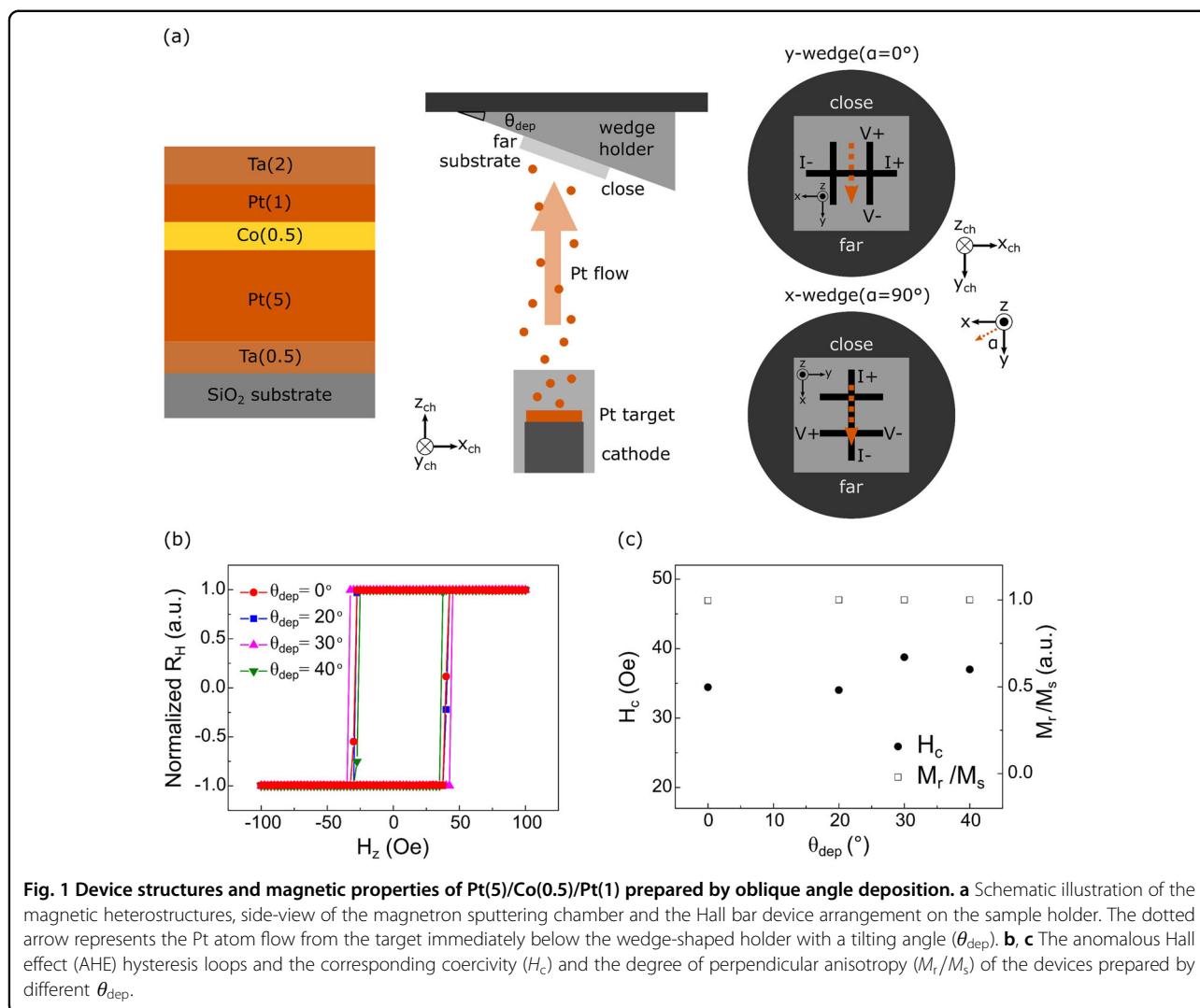


**Fig. 1** Device structures and magnetic properties of Pt(5)/Co(0.5)/Pt(1) prepared by oblique angle deposition. **a** Schematic illustration of the magnetic heterostructures, side-view of the magnetron sputtering chamber and the Hall bar device arrangement on the sample holder. The dotted arrow represents the Pt atom flow from the target immediately below the wedge-shaped holder with a tilting angle ( $\theta_{dep}$ ). **b, c** The anomalous Hall effect (AHE) hysteresis loops and the corresponding coercivity ( $H_c$ ) and the degree of perpendicular anisotropy ( $M_r/M_s$ ) of the devices prepared by different  $\theta_{dep}$ .

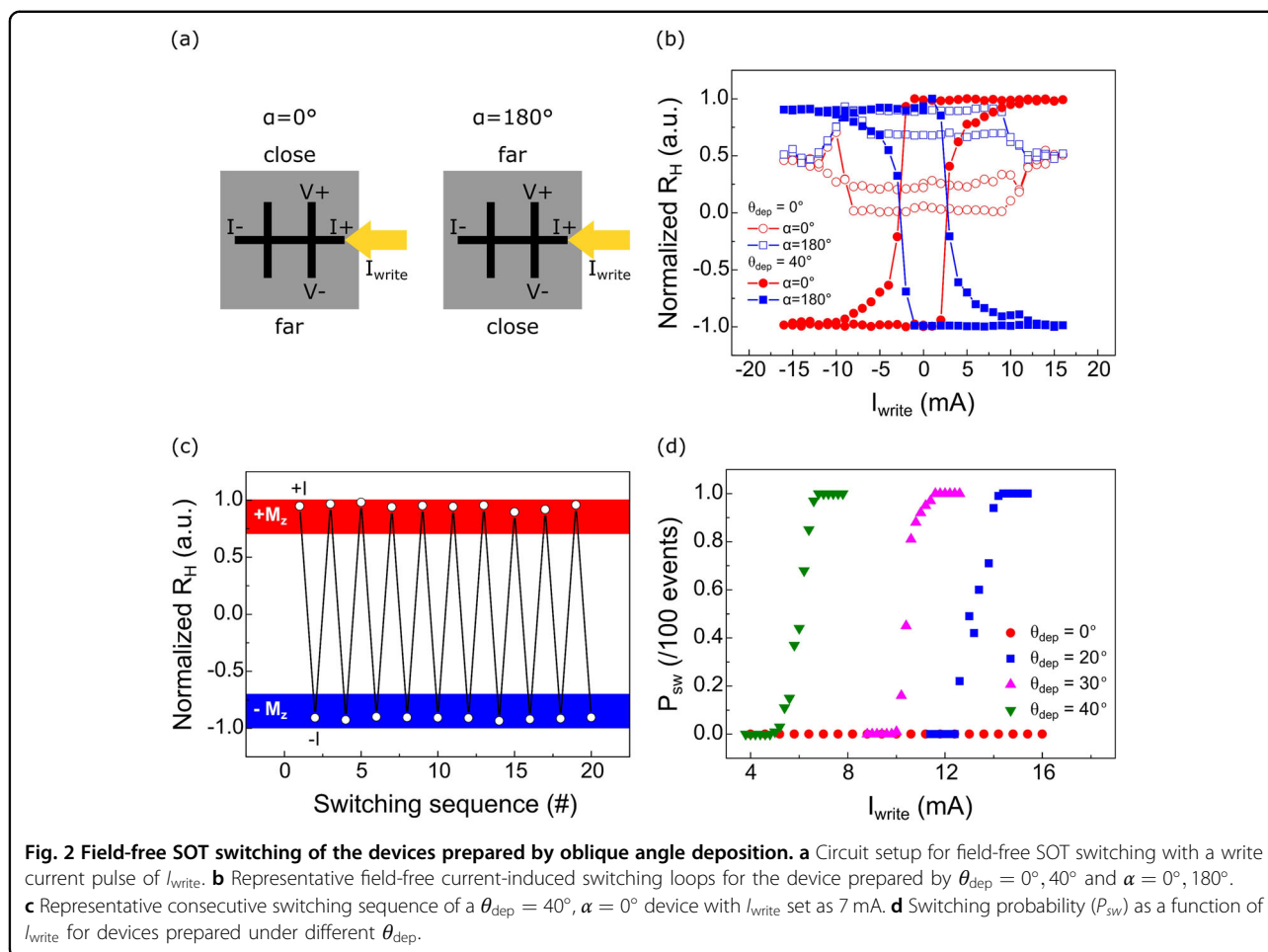
magnetization under zero external field and the saturated magnetization is defined by the normalized  $R_H$  under  $H_z = 0$  Oe ( $M_r/M_s \equiv R_H^{H_z=0\text{Oe}}/R_H^{\text{max}}$ ) and is used as a figure of merit for evaluating PMA. The out-of-plane  $H_c$  and  $M_r/M_s$  for each  $\theta_{dep}$  condition are summarized in Fig. 1c, showing that the  $H_c$  (ranging from 30 to 40 Oe) and the PMA properties are largely insensitive to the varying  $\theta_{dep}$  in these Hall bar devices. The estimated DL-SOT efficiency ( $\xi_{DL}$ ) and the out-of-plane anisotropy field ( $H_k$ ) are also demonstrated to be not strongly affected by varying  $\theta_{dep}$  (see Supporting Information S2 and S3).

## Results

### Demonstration of robust field-free switching in obliquely deposited Pt/Co/Pt structures

The experimental setup for field-free switching is schematically shown in Fig. 2a. The switching sequence consists of alternatively applying a write current pulse ( $I_{write}$ ) of various amplitudes and a read current pulse

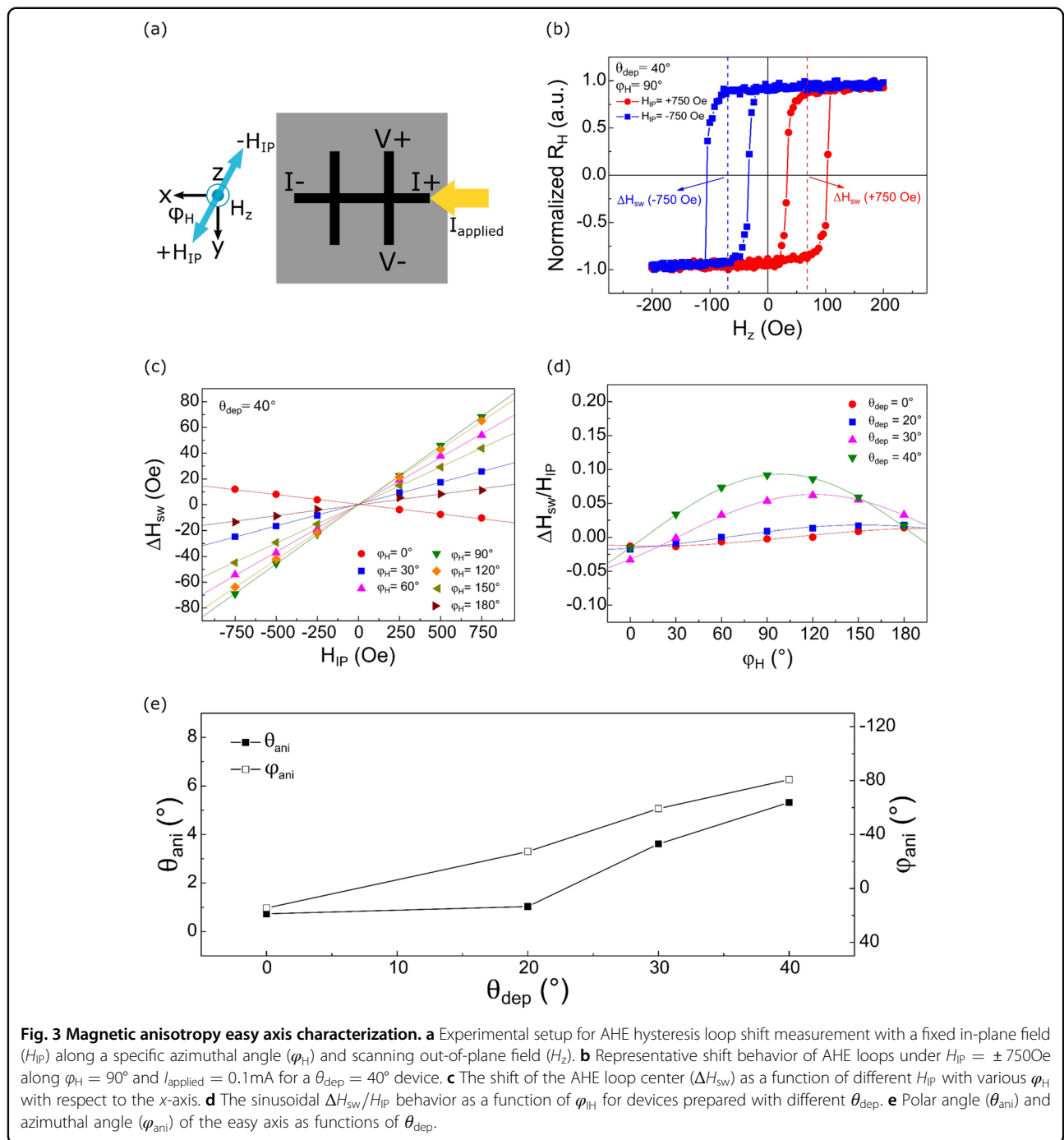
( $I_{read}$ ) of 0.1 mA into the Hall bar devices to alter and read out the magnetization state through the AHE. The pulse width ( $t_{pulse}$ ) is set as 0.05 s. These experiments were conducted in an external-field-free condition (probe station without electromagnets). Figure 2b shows representative field-free switching loops for the devices prepared under  $\theta_{dep} = 0^\circ, 40^\circ$  and  $\alpha = 0^\circ, 180^\circ$ . For the case of  $\theta_{dep} = 0^\circ$ , both  $\alpha = 0^\circ$  and  $180^\circ$  devices are not capable of achieving full switching ( $R_H$  differences in cases of field sweeping and current sweeping are nearly identical) under field-free conditions. However, full switching loops with opposite polarities can be observed in the case of  $\alpha = 0^\circ, 180^\circ$  prepared under  $\theta_{dep} = 40^\circ$ . To confirm the deterministic characteristics of these field-free switching loops, we further characterized the switching probabilities ( $P_{sw} \equiv \frac{\text{successful switching events}}{\text{total switching events}}$ ) of the devices prepared under  $\alpha = 0^\circ$  and different  $\theta_{dep}$ . Within each potential switching event, a sequence of  $+I_{write}$ ,  $+I_{read}$ ,  $-I_{write}$ , and  $+I_{read}$



pulses are applied to the device. A successful switching event is realized when the corresponding normalized  $R_H$  is over  $\pm 0.7$  after applying  $\pm I_{\text{write}}$ , as represented by the colored regions in Fig. 2c.  $P_{\text{sw}}$  (per 100 switching events) vs.  $I_{\text{write}}$  for devices with various  $\theta_{\text{dep}}$  are summarized in Fig. 2d. The zero-switching probability for the  $\theta_{\text{dep}} = 0^\circ$  device indicates that the nonwedge structure cannot realize field-free switching, as expected. In contrast, devices prepared by oblique angle deposition can achieve 100%  $P_{\text{sw}}$ . Furthermore, a clear reduction in  $I_{\text{write}}$  to reach full deterministic switching is observed by increasing  $\theta_{\text{dep}}$ : 14.4 mA for  $\theta_{\text{dep}} = 20^\circ$ , 11.6 mA for  $\theta_{\text{dep}} = 30^\circ$ , and 6.8 mA for  $\theta_{\text{dep}} = 40^\circ$ . This result indicates that the spin torque response enforced on the Co layer can be tuned by adjusting  $\theta_{\text{dep}}$ , which could originate from the change in magnetic properties (such as a tilted easy axis of magnetization) or the change in the spin current generation mechanism (structure-dependent unconventional spin current). The abovementioned current-induced field-free switching can be observed for a wide range of applied current pulse widths,  $30\mu\text{s} < t_{\text{pulse}} < 900\text{ms}$ , from which

the switching is determined to be in the thermally activated regime (details in Supporting Information S4). Additionally, by using a two-step fabrication process, we identified that the oblique angle deposition of the bottom Pt layer, while compared to other layers, plays a more decisive role in realizing field-free current-induced switching (see Supporting Information S5). Such two-step fabricated samples might also experience some level of interfacial oxidation, which can potentially enhance the overall DL-SOT efficiency<sup>37,38</sup>.

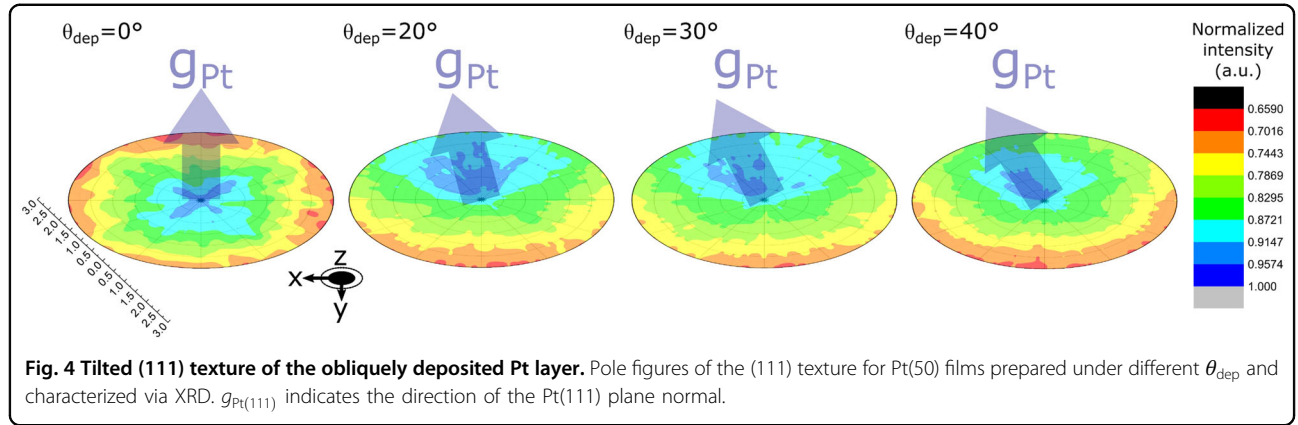
The observed field-free switching behavior is also found to be fairly uniform across millimeter (mm)-scale with different devices prepared on the same piece of substrate (details in Supporting Information S6). However, in industrial applications, a primary challenge impeding the effectiveness of techniques utilizing oblique angle deposition is the uneven thickness distribution (in this case, the Pt layer) across the entire 200 mm or 300 mm wafer. We propose that the integration of this field-free switching solution on a wafer scale could become feasible in the future if large-scale, uniform Pt films can be deposited in an oblique fashion.



### Evaluation of the tilted magnetic anisotropy

We first examined the possibility of having tilted easy axes in these samples with nonzero  $\theta_{dep}$ . To characterize such potentially minute changes in the easy axis direction, we adopted modified AHE hysteresis loop shift measurements with in-plane magnetic field  $H_{IP}$  scanning along various azimuthal angles  $\varphi_H$ <sup>18,22</sup>, as shown in Fig. 3a. The working principle of this measurement is that if the easy axis tilts away from the  $z$ -axis, the nonzero

component of the applied external in-plane field projected onto the easy axis would lead to a shift in the out-of-plane hysteresis loop while sweeping  $H_z$ ; in contrast, no shift will be observed in the case of the easy axis lying exactly on the  $z$ -axis. To prevent sizable contributions from the Joule heating and spin torque effects, the longitudinal sense current to generate the Hall voltage is set as 0.1 mA. Representative AHE data obtained from a  $\theta_{dep} = 40^\circ$  device are shown in Fig. 3b, from which a clear shift in



the out-of-plane hysteresis loop (denoted as  $\Delta H_{\text{sw}}$ ) is observed under  $H_{\text{IP}} = 750$  Oe and  $\varphi_{\text{H}} = 90^\circ$ .

The exact direction of the tilted easy axis, which is parameterized by  $\theta_{\text{ani}}$  and  $\varphi_{\text{ani}}$  (the polar and azimuthal angles), can be estimated from the loop shift results as follows. First, the sum of the externally applied in-plane fields along the easy axis ( $H_{\text{ea}}$ ) is:

$$H_{\text{ea}} = H_z \cos \theta_{\text{ani}} + H_{\text{IP}} \cos(\varphi_{\text{ani}} - \varphi_{\text{H}}) \sin \theta_{\text{ani}}. \quad (1)$$

Since the switching fields along the easy axis should be the same for DOWN-to-UP and UP-to-DOWN transitions ( $H_{\text{ea}}^{\text{DN-to-UP}} = -H_{\text{ea}}^{\text{UP-to-DN}}$ ), the shift of the AHE hysteresis loop center  $\Delta H_{\text{sw}} \equiv \frac{1}{2}(H_{\text{sw}}^{\text{UP-to-DN}} + H_{\text{sw}}^{\text{DN-to-UP}})$  obtained experimentally is therefore linearly proportional to  $H_{\text{IP}}$ :

$$\begin{aligned} \frac{\Delta H_{\text{sw}}}{H_{\text{IP}}} &\equiv \frac{H_z^{\text{DN-to-UP}} + H_z^{\text{UP-to-DN}}}{2H_{\text{IP}}} \\ &= -\cos(\varphi_{\text{ani}} - \varphi_{\text{H}}) \tan \theta_{\text{ani}}, \end{aligned} \quad (2)$$

where  $H_z^{\text{DN-to-UP}}$  and  $H_z^{\text{UP-to-DN}}$  are the switching fields extracted from the AHE hysteresis loops. Such a linear relationship under different  $\varphi_{\text{H}}$  for a  $\theta_{\text{dep}} = 40^\circ$  device is shown in Fig. 3c. The values of  $\theta_{\text{ani}}$  and  $\varphi_{\text{ani}}$  can then be extracted by fitting  $\frac{\Delta H_{\text{sw}}}{H_{\text{IP}}}$  vs.  $\varphi_{\text{H}}$  using Eq. (2), as shown in Fig. 3d.

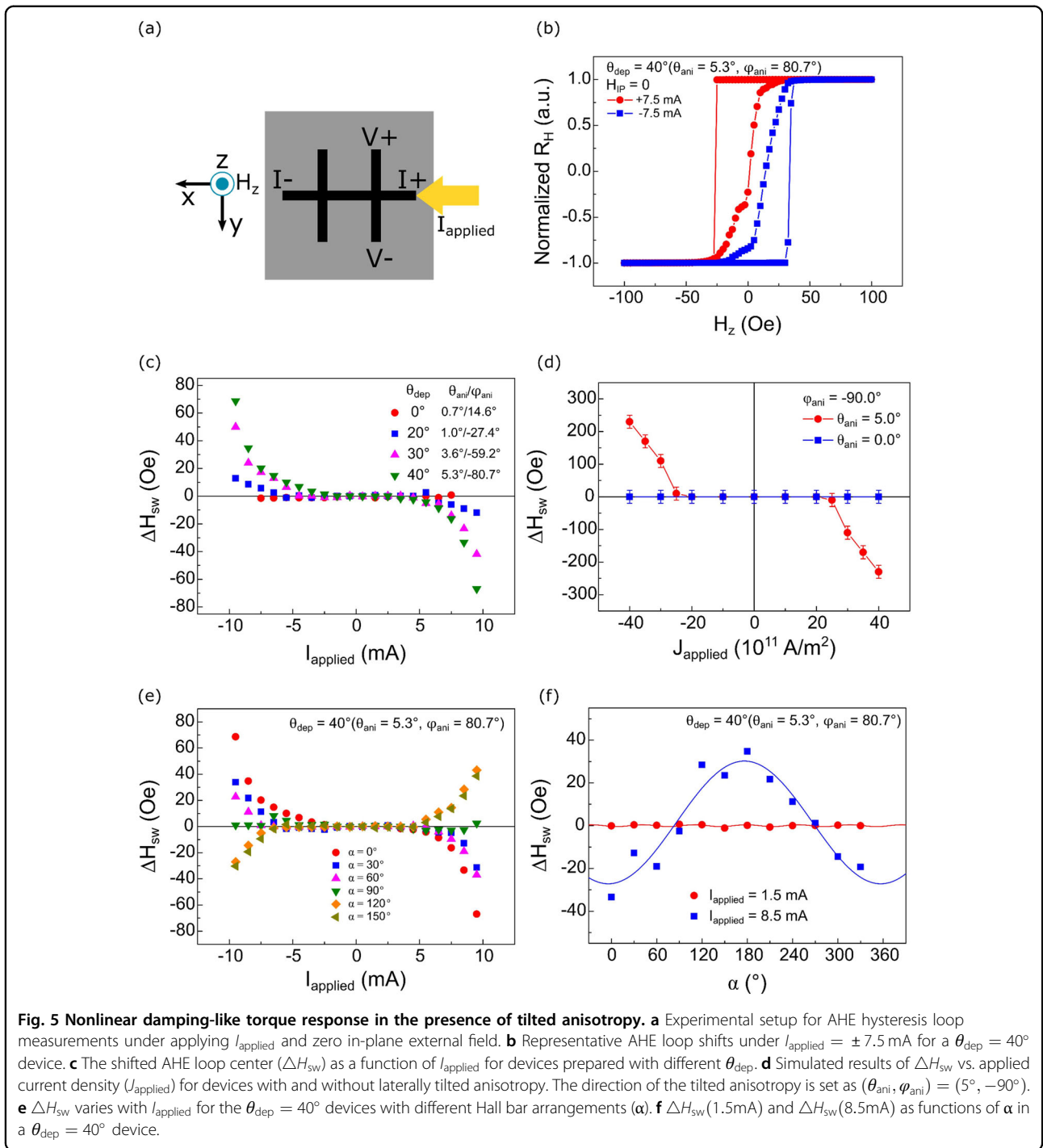
We summarize the oblique deposition angle  $\theta_{\text{dep}}$  dependence of the tilted easy axis ( $\theta_{\text{ani}}$ ,  $\varphi_{\text{ani}}$ ) in Fig. 3e. The negligible  $\theta_{\text{ani}}$  and  $\varphi_{\text{ani}}$  for the control sample prepared under  $\theta_{\text{dep}} = 0^\circ$  indicates a typical PMA behavior in which the easy axis is fairly close to the z-axis ( $\theta_{\text{ani}} = 0.74^\circ$  and  $\varphi_{\text{ani}} = 14.57^\circ$ ). For the devices prepared by oblique angle deposition,  $\theta_{\text{ani}}$  gradually increases as  $\theta_{\text{dep}}$  increases ( $\theta_{\text{ani}} = 5.32^\circ$  for  $\theta_{\text{dep}} = 40^\circ$ ). The easy axis also gradually points toward the y-axis when using a larger  $\theta_{\text{dep}}$  ( $\varphi_{\text{ani}} = -80.73$  for  $\theta_{\text{dep}} = 40^\circ$ ). The origin of this tilted anisotropy is attributed to the tilted (111) texture observed in the Pt films prepared by oblique angle

deposition, which is quite different from the normal (111) texture observed from the  $\theta_{\text{dep}} = 0^\circ$  films.

To showcase the existence of such a tilted texture, pole figures of various 50 nm thick Pt films characterized by XRD are shown in Fig. 4. The Pt(111) peak is normal to the film surface for the Pt film prepared by  $\theta_{\text{dep}} = 0^\circ$ . In sharp contrast, those prepared by oblique deposition  $\theta_{\text{dep}} > 0^\circ$  show tilted Pt(111) textures with the Pt(111) normal tilting toward the  $-y$  direction. Furthermore, the easy axis direction of those samples prepared by two-step fabrication shown in Supporting Information S5 also supports the correlation between tilted anisotropy and tilted Pt(111) texture:  $\theta_{\text{ani}} = 5.14^\circ$  and  $\varphi_{\text{ani}} = -87.5^\circ$  for  $\theta_{\text{dep}} > 0^\circ$ , whereas  $\theta_{\text{ani}} = 0.52^\circ$  and  $\varphi_{\text{ani}} = 41.9^\circ$  for  $\theta_{\text{dep}} = 0^\circ$ . These results again confirm that the tilted (111) texture of the underlayer Pt originating from oblique angle deposition can induce a tilted anisotropy of the neighboring Co layer. Such a correlation between the crystalline texture and anisotropy can be explained by the fact that the PMA in Pt/Co systems strongly relies on the formation of a Pt(111) texture<sup>39,40</sup>. Note that this mechanism is different from the one attributed to the Co thickness gradient<sup>18</sup> since the Co layer in this work was grown uniformly. Additionally, note that the polycrystalline nature of the sputter-deposited Pt also rules out the possibility of producing any sizable unconventional spin currents related to the broken crystal symmetry<sup>41</sup>.

#### Current-driven field-free SOT switching: conventional DL-SOT plus tilted anisotropy

To further investigate the origin of field-free current-induced switching under tilted anisotropy, current-induced AHE hysteresis loop shift measurements were conducted in an in-plane-field-free probe station, as illustrated in Fig. 5a. Using this approach, we can obtain the out-of-plane AHE loop shift  $\Delta H_{\text{sw}} \equiv \frac{1}{2}(H_{\text{sw}}^{\text{UP-to-DN}} + H_{\text{sw}}^{\text{DN-to-UP}})$  as a function of applied current ( $I_{\text{applied}}$ ), ranging from  $-9.5$  mA to



+9.5 mA in the absence of  $H_{\text{IP}}$ . Representative current-induced AHE loop shift results for a  $\theta_{\text{dep}} = 40^\circ$  device under  $I_{\text{applied}} = \pm 7.5$  mA are shown in Fig. 5b. A clear DL (anti-damping) torque switching behavior is identified: the SOT only affects one of the magnetization switching fields  $H_{\text{sw}}$ , either that for DOWN-to-UP or UP-to-DOWN transition. Such behavior is not observed in the control sample with  $\theta_{\text{dep}} = 0^\circ$  (details of the switching fields of  $\theta_{\text{dep}} = 0^\circ$

and  $\theta_{\text{dep}} = 40^\circ$  under different  $I_{\text{applied}}$  can be found in Supporting Information S7).

More importantly, the AHE loop shifts  $\Delta H_{\text{sw}}$  vs.  $I_{\text{applied}}$ , as summarized in Fig. 5c, show clear nonlinear trends:  $\Delta H_{\text{sw}}$  is negligible in the small current regime, and a sizable  $\Delta H_{\text{sw}}$  is observed when the applied current exceeds a threshold value. This feature indicates that a large current is needed to activate the anti-damping

torque for field-free switching, which is considered evidence of the existence of a spin polarization component partially parallel to the magnetization, similar to the case regarding a spin current with  $z$ -spin polarization<sup>24</sup>. However, in our case, the parallel amount is related to the anisotropy tilt toward the  $y$ -axis, where  $\sigma \cdot \hat{m} = \sigma \sin \theta_{\text{ani}}$  per spin angular momentum ( $\sigma$ ). The spin polarization here is still conventional, i.e.,  $y$ -spin. Notably, this nonlinear torque response has already been observed and speculated as a result of tilted anisotropy in a previous work<sup>34</sup>, but the existence of a tilted anisotropy and the switching field feature of a conventional DL torque behavior have not been fully addressed and verified. Here, we unambiguously demonstrate that a conventional  $y$ -spin-polarization-induced DL-SOT plus tilted anisotropy scenario should be sufficient to explain the observed field-free switching.

The proposed mechanism is further verified via microspin simulation based on the UberMag package<sup>42</sup> (with OOMMF<sup>43</sup> as the kernel) to model current-induced hysteresis loop shifts  $\Delta H_{\text{sw}}$  under different applied current densities and anisotropy conditions. The modeled device size is set as  $720 \times 120 \times 1 \text{ nm}^3$  and is discretized by using a cuboid-shaped cell of  $4 \times 4 \times 1 \text{ nm}^3$  with uniform anisotropy energy of  $8 \times 10^5 \text{ J/cm}^3$ , DMI energy of  $1 \text{ J/m}^2$  and exchange energy of  $16 \times 10^{-12} \text{ J/m}$ . The spin Hall angle ( $\theta_{\text{SH}}$ ) is set to 0.2 with a conventional spin polarization along the  $y$ -axis. As shown in Fig. 5d,  $\Delta H_{\text{sw}}$  remains zero under various current densities  $J_{\text{applied}}$  for the  $\theta_{\text{ani}} = 0^\circ$  configuration, which is consistent with the net SOT being zero without the application of a longitudinal in-plane magnetic field. In the case with a laterally tilted anisotropy ( $\theta_{\text{ani}} = 5^\circ$ ,  $\varphi_{\text{ani}} = -90^\circ$ ), a clear threshold behavior of  $\Delta H_{\text{sw}}$  vs.  $J_{\text{applied}}$  agrees well with the abovementioned experimental results and again verifies the nonlinear DL torque response in a system with tilted anisotropy. Unconventional spins along the  $z$ -direction do not need to be included to reproduce such nonlinear features.

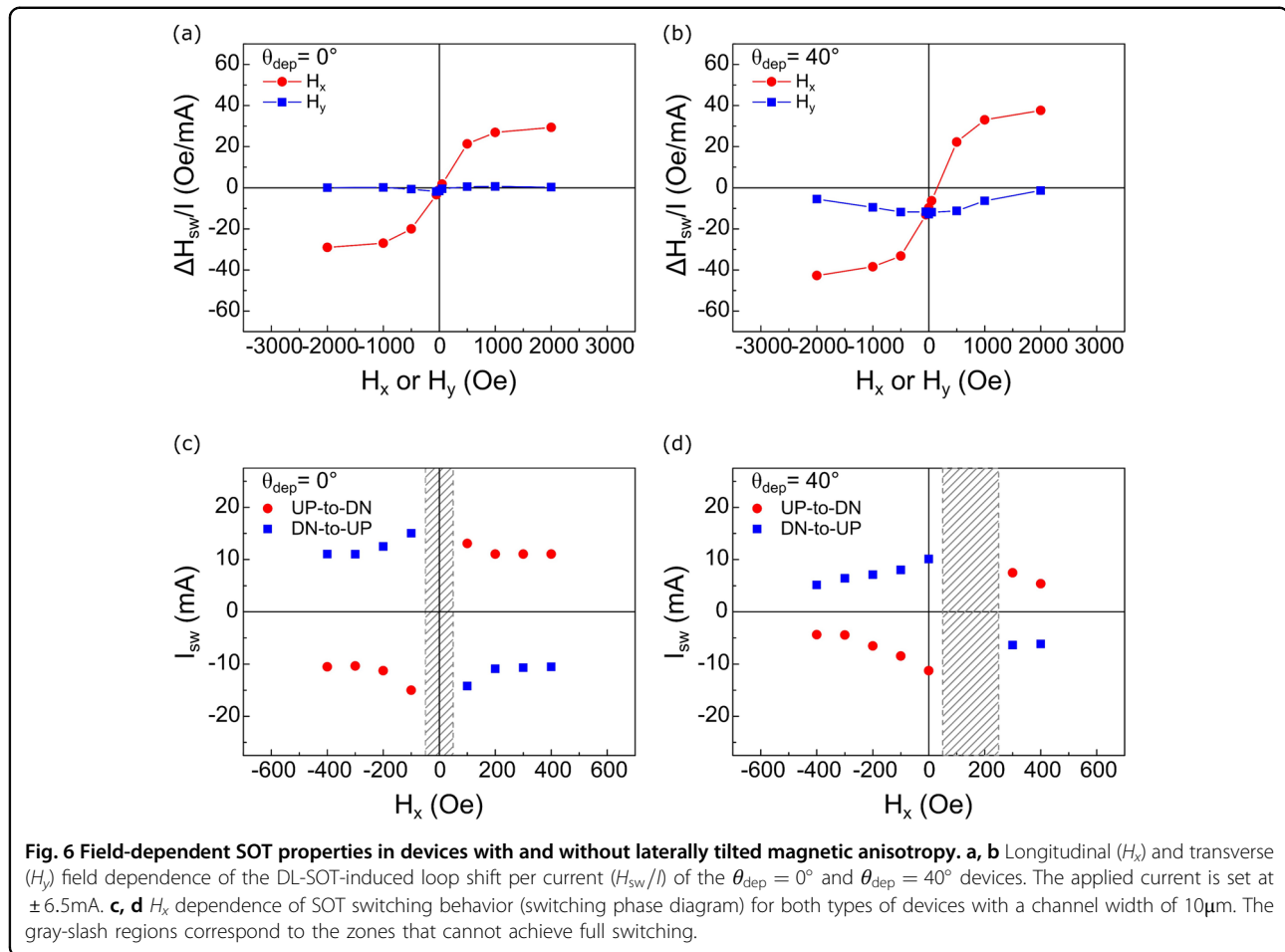
Additionally, as presented in Fig. 5e, such nonlinear  $\Delta H_{\text{sw}}$  vs.  $I_{\text{applied}}$  behavior can be controlled by the direction of oblique angle deposition  $\alpha$ . The  $\alpha$ -dependence of  $\Delta H_{\text{sw}}$  shown in Fig. 5f also indicates that the largest  $\Delta H_{\text{sw}}$  occurs when using oblique angle deposition along the transverse direction ( $\alpha = 0^\circ$ ), while  $\Delta H_{\text{sw}} \approx 0 \text{ Oe}$  for the longitudinally deposited device ( $\alpha = 90^\circ$ ). A clear sinusoidal trend is observed (absent) in the case of a large (small) applied current, indicating that the Pt(111) texture and the corresponding tilted anisotropy direction are controlled by  $\theta_{\text{dep}}$  and the sufficient current for anti-damping torque activation, both of which are important for the observation of this nonlinear response in the absence of an in-plane field.

### Longitudinal effective in-plane field in the presence of tilted anisotropy

Next, we examine and compare the difference in the field-dependent SOT responses between devices with and without tilted anisotropy by both conventional current-induced hysteresis loop shift and current-induced SOT switching measurements in the presence of an externally applied in-plane field. The applied current in the hysteresis loop shift measurement is set at  $\pm 6.5 \text{ mA}$  to reflect the behavior within the activation regime, and the corresponding results are summarized in Fig. 6a, b. For the case without tilted anisotropy, a classical trend<sup>16</sup> of the perpendicular effective field per current ( $\Delta H_{\text{sw}}/I$ ) is observed as expected: when applying a longitudinal external field along the  $x$ -axis,  $H_x$ , the magnitude of  $\Delta H_{\text{sw}}/I$  starts to increase from zero and then saturates. No observable trend in  $\Delta H_{\text{sw}}/I$  appears when applying a transverse external field ( $H_y$ ) due to the absence of domain expansion/shrinkage in the Bloch-type-like domain wall geometry. In contrast, these behaviors become quite different when a tilted anisotropy is introduced into the system: A finite  $\Delta H_{\text{sw}}/I$  in the zero  $H_{x(y)}$  condition is observed for the  $\theta_{\text{dep}} = 40^\circ$  device (Fig. 6b), which contributes to the field-free switching when applying a sufficient amount of current into the device. Moreover, the overall  $\Delta H_{\text{sw}}/I$  vs.  $H_x$  relationship shows a clear shift in the longitudinal direction and can be suppressed as  $H_x$  reaches approximately 150 Oe, indicating that the outcome of the laterally tilted anisotropy can be phenomenologically viewed as a negative longitudinal effective field.

The presence of this effective field, which is orthogonal to the spin polarization direction and the tilted easy axis, can be attributed to the emergence of DL-SOT as the magnetization  $m$  is activated and lies in the hard plane. Without tilted anisotropy, such a DL-SOT effective field is proportional to  $m \times \sigma = 0$  or parallel to the  $z$ -axis, thereby missing the in-plane field component. However, with a laterally tilted anisotropy, the DL-SOT effective field experienced by the magnetization within the hard plane is nonzero and along  $m \times \sigma \parallel \hat{x}$ . In our case of having a conventional  $y$ -axis spin polarization ( $\sigma \parallel \mp \hat{y}$ ) carried by a positive (negative) charge current in the Pt layer (along the  $x$ -axis),  $m$  lying within the negative (positive)  $yz$ -plane would both experience a negative DL-SOT effective field pointing along  $x$ . This characteristic is also reported in a similar system with a canted easy axis, albeit having in-plane anisotropy<sup>44</sup>. Additionally, note that this finite zero-in-plane-field  $\Delta H_{\text{sw}}/I$  can be suppressed by applying a large enough  $\pm H_y$ , since the activated magnetization would eventually be aligned with the spin polarization direction and result in a zero DL-SOT effective field ( $m \times \sigma = 0$ ).





Finally, we show the switching phase diagrams for both control and tilted anisotropy devices in Fig. 6c, d. Without tilted anisotropy, the switching phase diagram is symmetric to the origin and misses the deterministic switching behavior under field-free conditions, as expected. After introducing the laterally tilted anisotropy, a clear shift along the longitudinal field direction is observed, which is consistent with the hysteresis loop shift measurements and again verifies the existence of a phenomenological longitudinal DL-SOT effective field.

## Conclusion

In this work, we systematically investigate current-induced field-free SOT switching in Pt/Co/Pt magnetic heterostructures with PMA. Deterministic, robust field-free switching are achieved in devices with underlayer Pt layers prepared by oblique angle deposition, and the switching current in such devices can be reduced by tuning the deposition angle. We further verify that the mechanism of such field-free switching being magnetic symmetry breaking originated from the laterally tilted anisotropy, which is correlated to the tilted (111) texture of the underlayer Pt.

We also demonstrate experimentally and in simulation that the nonlinear current dependence of DL torque-induced  $\Delta H_{sw}$  is an important feature for such a “conventional DL-SOT plus tilted anisotropy” scenario. Additionally, the existence of a longitudinal effective field in the switching phase diagram is another key feature within this scheme, which results from the nonzero longitudinal component of the DL-SOT effective field when activating upon magnetization. Our work therefore highlights the critical role of anisotropy engineering in realizing field-free SOT switching of perpendicular magnetization.

## Acknowledgements

This study is financially supported by the National Science and Technology Council of Taiwan (NSTC) under grant No. NSTC 112-2636-M-002-006 and by the Center of Atomic Initiative for New Materials (AIMat), National Taiwan University from the Featured Areas Research Center Program within the framework of the Higher Education Sprout Project by the Ministry of Education (MOE) in Taiwan under grant No. NTU-112L9008.

## Author details

<sup>1</sup>Department of Materials Science and Engineering, National Taiwan University, Taipei 10617, Taiwan. <sup>2</sup>Center of Atomic Initiative for New Materials, National Taiwan University, Taipei 10617, Taiwan. <sup>3</sup>Center for Quantum Science and Engineering, National Taiwan University, Taipei 10617, Taiwan

**Author contributions**

C.Y.H. and W.D.C. contributed equally to this work. C.F.P. proposed and supervised the study. C.Y.H. and W.D.C. designed and fabricated the samples. C.Y.H. and W.D.C. performed the electrical measurements with assistance from C.C.H. for using the vector field probe station. Y.T.L. performed the magnetic simulations. C.Y.H. performed the XRD pole figure characterizations. C.Y.H. and W.D.C. drafted the manuscript with input from all coauthors.

**Conflict of interest**

The authors declare no competing interests.

**Publisher's note**

Springer Nature remains neutral with regard to jurisdictional claims in published maps and institutional affiliations.

**Supplementary information** The online version contains supplementary material available at <https://doi.org/10.1038/s41427-023-00521-9>.

Received: 7 May 2023 Revised: 1 November 2023 Accepted: 9 November 2023

Published online: 12 January 2024

**References**

- Liu, L. Q. et al. Spin-torque switching with the giant spin hall effect of tantalum. *Science* **336**, 555–558 (2012).
- Garello, K. et al. Symmetry and magnitude of spin-orbit torques in ferromagnetic heterostructures. *Nat. Nanotechnol.* **8**, 587–593 (2013).
- Miron, I. M. et al. Current-driven spin torque induced by the Rashba effect in a ferromagnetic metal layer. *Nat. Mater.* **9**, 230–234 (2010).
- Cubukcu, M. et al. Ultra-Fast Perpendicular Spin-Orbit Torque MRAM. *IEEE Trans. Magn.* **54**, 9300204 (2018).
- Dieny, B. et al. Opportunities and challenges for spintronics in the microelectronics industry. *Nat. Electron.* **3**, 446–459 (2020).
- Sinova, J., Valenzuela, S. O., Wunderlich, J., Back, C. H. & Jungwirth, T. Spin Hall effects. *Rev. Mod. Phys.* **87**, 1213–1259 (2015).
- Hu, C. Y. & Pai, C. F. Benchmarking of spin-orbit torque switching efficiency in Pt alloys. *Adv. Quantum Technologies* 2000024 (2020).
- Hu, C.-Y. et al. Toward 100% spin-orbit torque efficiency with high spin-orbital hall conductivity Pt-Cr alloys. *ACS Appl. Electron. Mater.* **4**, 1099–1108 (2022).
- Edelstein, V. M. Spin polarization of conduction electrons induced by electric current in two-dimensional asymmetric electron systems. *Solid State Commun.* **73**, 233–235 (1990).
- Rojas Sanchez, J. C. et al. Spin-to-charge conversion using Rashba coupling at the interface between non-magnetic materials. *Nat. Commun.* **4**, 2944 (2013).
- Slonczewski, J. C. Current-driven excitation of magnetic multilayers. *J. Magn. Magn. Mater.* **159**, L1–L7 (1996).
- Berger, L. Emission of spin waves by a magnetic multilayer traversed by a current. *Phys. Rev. B* **54**, 9353–9358 (1996).
- Ikeda, S. et al. A perpendicular-anisotropy CoFeB-MgO magnetic tunnel junction. *Nat. Mater.* **9**, 721–724 (2010).
- Haazen, P. P. J. et al. Domain wall depinning governed by the spin Hall effect. *Nat. Mater.* **12**, 299–303 (2013).
- Emori, S., Bauer, U., Ahn, S. M., Martinez, E. & Beach, G. S. D. Current-driven dynamics of chiral ferromagnetic domain walls. *Nat. Mater.* **12**, 611–616 (2013).
- Pai, C. F., Mann, M., Tan, A. J. & Beach, G. S. D. Determination of spin torque efficiencies in heterostructures with perpendicular magnetic anisotropy. *Phys. Rev. B* **93**, 144409 (2016).
- Garello, K. et al. Manufacturable 300mm platform solution for Field-Free Switching SOT-MRAM. In: *2019 Symposium on VLSI Circuits T194-T195* (IEEE, 2019). <https://doi.org/10.23919/VLSIT.2019.876537>.
- Mohanani, P. V., Ganesh, K. R. & Kumar, P. S. A. Spin Hall effect mediated current-induced deterministic switching in all-metallic perpendicularly magnetized Pt/Co/Pt trilayers. *Phys. Rev. B* **96**, 104412 (2017).
- You, L. et al. Switching of perpendicularly polarized nanomagnets with spin orbit torque without an external magnetic field by engineering a tilted anisotropy. *Proc. Natl Acad. Sci. USA* **112**, 10310–10315 (2015).
- Liu, L. et al. Current-induced magnetization switching in all-oxide heterostructures. *Nat. Nanotechnol.* **14**, 939–944 (2019).
- Kim, H. J. et al. Field-free switching of magnetization by tilting the perpendicular magnetic anisotropy of Gd/Co multilayers. *Adv. Funct. Mater.* **32**, 2112561 (2022).
- Chang, M. X. et al. Field free magnetization switching in perpendicularly magnetized Pt/Co/FeNi/Ta structure by spin orbit torque. *Appl. Phys. Lett.* **117**, 142404 (2020).
- Liu, L. et al. Symmetry-dependent field-free switching of perpendicular magnetization. *Nat. Nanotechnol.* **16**, 277–282 (2021).
- Baek, S. H. C. et al. Spin currents and spin-orbit torques in ferromagnetic trilayers. *Nat. Mater.* **17**, 509–513 (2018).
- Ma, Q. et al. Switching a perpendicular ferromagnetic layer by competing spin currents. *Phys. Rev. Lett.* **120**, 117703 (2018).
- Chu, R. et al. Electrical control of spin hall efficiency and field-free magnetization switching in W/Pt/Co/Pt heterostructures with competing spin currents. *ACS Appl. Mater. Interfaces* **15**, 29525–29534 (2023).
- Yu, G. Q. et al. Current-driven perpendicular magnetization switching in Ta/CoFeB/(TaO<sub>x</sub> or MgO/TaO<sub>x</sub>) films with lateral structural asymmetry. *Appl. Phys. Lett.* **105**, 102411 (2014).
- Lau, Y. C., Betto, D., Rode, K., Coey, J. M. D. & Stamenov, P. Spin-orbit torque switching without an external field using interlayer exchange coupling. *Nat. Nanotechnol.* **11**, 758–762 (2016).
- Huang, Y.-H., Huang, C.-C., Liao, W.-B., Chen, T.-Y. & Pai, C.-F. Growth-Dependent Interlayer Chiral Exchange and Field-Free Switching. *Phys. Rev. Appl.* **18**, 034046 (2022).
- Oh, Y. W. et al. Field-free switching of perpendicular magnetization through spin-orbit torque in antiferromagnet/ferromagnet/oxide structures. *Nat. Nanotechnol.* **11**, 878–884 (2016).
- Fukami, S., Zhang, C. L., DuttaGupta, S., Kurenkov, A. & Ohno, H. Magnetization switching by spin-orbit torque in an antiferromagnet-ferromagnet bilayer system. *Nat. Mater.* **15**, 535–541 (2016).
- Murray, N. et al. Field-free spin-orbit torque switching through domain wall motion. *Phys. Rev. B* **100**, 104441 (2019).
- Shu, X. Y. et al. Field-free switching of perpendicular magnetization induced by longitudinal spin-orbit-torque gradient. *Phys. Rev. Appl.* **17**, 024031 (2022).
- Torrejon, J. et al. Current-driven asymmetric magnetization switching in perpendicularly magnetized CoFeB/MgO heterostructures. *Phys. Rev. B* **91**, 214434 (2015).
- Huang, C. C., Tsai, C. C., Liao, W. B., Chen, T. Y. & Pai, C. F. Deep learning for spin-orbit torque characterizations with a projected vector field magnet. *Phys. Rev. Res.* **4**, 033040 (2022).
- Nagaosa, N., Sinova, J., Onoda, S., MacDonald, A. H. & Ong, N. P. Anomalous Hall effect. *Rev. Mod. Phys.* **82**, 1539–1592 (2010).
- Qiu, X. et al. Spin-orbit-torque engineering via oxygen manipulation. *Nat. Nanotechnol.* **10**, 333–338 (2015).
- Zhao, T. et al. Enhancement of out-of-plane spin-orbit torque by interfacial modification. *Adv. Mater.* **35**, 2208954 (2023).
- Parakkat, V. M., Ganesh, K. R. & Kumar, P. S. A. Tailoring Curie temperature and magnetic anisotropy in ultrathin Pt/Co/Pt films. *Aip Adv.* **6**, 056118 (2016).
- Carcia, P. F., Li, Z. G. & Zeper, W. B. Effect of sputter-deposition processes on the microstructure and magnetic-properties of Pt/Co multilayers. *J. Magn. Magn. Mater.* **121**, 452–460 (1993).
- Liu, Y. T. & Shao, A. M. Two-dimensional materials for energy-efficient spin-orbit torque devices. *ACS Nano* **14**, 9389–9407 (2020).
- Beg, M., Lang, M. & Fangohr, H. Ubermag: toward more effective micro-magnetic workflows. *IEEE Trans. Magn.* **58**, 7300205 (2022).
- Donahue, M. OOMMF User's Guide, Version 1.0, - 6376, National Institute of Standards and Technology, Gaithersburg, MD (1999). <https://doi.org/10.6028/NIST.JR.6376>.
- Liu, Y. T. et al. Field-free type-x spin-orbit-torque switching by easy-axis engineering. *Phys. Rev. Appl.* **18**, 034019 (2022).